

Inertial migration of oblate spheroids in a plane channel

Tatiana V. Nizkaya,¹ Anna S. Gekova,¹ Jens Harting,^{2,3} Evgeny S. Asmolov,¹ and Olga I. Vinogradova^{1, a)}

¹*Frumkin Institute of Physical Chemistry and Electrochemistry, Russian Academy of Science, 31 Leninsky Prospekt, 119071 Moscow, Russia*

²*Helmholtz Institute Erlangen-Nürnberg for Renewable Energy, Forschungszentrum Jülich, Fürther Str. 248, 90429 Nürnberg, Germany*

³*Department of Chemical and Biological Engineering and Department of Physics, Friedrich-Alexander-Universität Erlangen-Nürnberg, Fürther Str. 248, 90429 Nürnberg, Germany*

(Dated: November 4, 2020)

We discuss an inertial migration of oblate spheroids in a plane channel, where steady laminar flow is generated by a pressure gradient. Our lattice Boltzmann simulations show that spheroids orient in the flow, so that their minor axis coincides with the vorticity direction (a log-rolling motion). Interestingly, for spheroids of moderate aspect ratios, the equilibrium positions relative to the channel walls depend only on their equatorial radius a . By analysing the inertial lift force we argue that this force is proportional to a^3b , where b is the polar radius, and conclude that the dimensionless lift coefficient of the oblate spheroid does not depend on b , and is equal to that of the sphere of radius a .

I. INTRODUCTION

It is well-known that at finite Reynolds numbers particles migrate across streamlines of the flow to some equilibrium positions in the microchannel. This migration is attributed to inertial lift forces, which are currently successfully used in microfluidic systems to focus and separate particles of different sizes continuously, which is important for a wide range of applications^{1,2}. The rapid development of an inertial microfluidics has raised a considerable interest in the lift forces on particles in confined flows. The majority of previous work on lift forces has assumed that particles are spherical. In their pioneering experiments, Segrè and Silberberg found that small spheres focus to a narrow annulus at a radial position of about 0.6 of a pipe radius³. Later, several theoretical⁴⁻⁷ and numerical⁸ studies proposed useful scaling and approximate expressions for the lift force in a channel flow, which are frequently invoked. The assumption that particles are spherical often becomes unrealistic. The non-sphericity could strongly modify the lift forces, so the shape of particles becomes a very important consideration⁹. The body of theoretical and experimental work investigating lift forces on non-spherical particles is much less than that for spheres, although there is a growing literature in this area.

Hur *et al.*¹⁰ and Masaeli *et al.*¹¹ appear to have been the first to study experimentally the inertial focusing of non-spherical particles. These authors addressed themselves to the case of particles (spheres and rods of different aspect ratios) of equal volume, and demonstrated the possibility of their separation in a planar channel of moderate Reynolds numbers, $Re \leq 100$. Roth *et al.*¹² recently reported the separation of spheres, ellipsoids and peanut-shaped particles in a spiral microfluidic device, where the inertial lift force is balanced by the Dean force that can be generated in curved channels¹³. These papers concluded that a key parameter defining equilibrium positions of particles is their rotational diameter. The

authors, however, could not relate their results neither to the variation of the lift force across the channel nor with its dependence on particle shape since these are inaccessible in experiment.

The theoretical analysis of the lift on non-spherical particles is beset with difficulties since they could vary their orientation due to a rotation in a shear flow, which, in turn, could induce unsteady flow disturbances leading to a time-dependent lift¹⁴. There have been some attempts to provide a theory of such a motion by employing spheroids as a simplest model for non-spherical particles. It is known that at vanishing particle Reynolds numbers, Re_p , non-inertial spheroids exhibit in a shear flow a periodic kayaking motion along one of the Jeffrey orbits¹⁵. However, the orientation of oblate spheroids of finite Re_p eventually tends to a stable state due to inertia of the fluid and the particle¹⁶.

Computer simulations might shed some light on these phenomena, and, indeed, computational inertial microfluidics is a growing field that currently attracts much research efforts¹⁷. There is a number of simulations using the lattice Boltzmann method (LBM) that is well-suited for parallel processing and allows one an efficient tracking of the particle-fluid interface¹⁸, which are directly relevant. A large fraction of these deal with rotation properties of spheroids in shear flows¹⁹⁻²². At moderate Re_p , oblate spheroids exhibit a log-rolling motion about their minor axis oriented along the vorticity direction, while prolate particles tumble, but when $Re_p > 200$, in some situations a transition to other rotational regimes may occur¹⁹. Its threshold depends on the particle aspect ratio, which can be used for their separation²³. However, neither this paper addresses itself to the issues of inertial migration. This was taken up only recently in the paper by Lashgari *et al.*²⁴, who carried out simulations of stable equilibrium positions and orientations of oblate spheroids in rectangular channels. The lift force on cylindrical particles in rectangular ducts has been calculated by Su, Chen, and Hu¹⁴. These authors found that particles execute a periodic tumbling motion, so that the lift force is unsteady, but its average dependence on the particle position, however, is similar to that for a sphere. Finally we should mention that Huang, Marson, and

^{a)}Corresponding author: oivinograd@yahoo.com

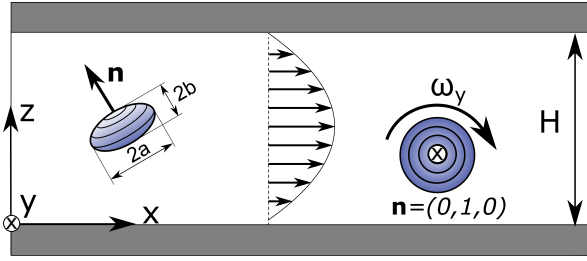


Figure 1. An oblate spheroid orienting in a pressure-driven flow to perform a stable log-rolling state.

Larson²⁵ used dissipative particle dynamics simulations to find the equilibrium positions for prolate and oblate spheroids in a plane Poiseuille flow.

Nevertheless, in spite of its importance for separations of particles, the connection between the shape of non-spherical particles and emerging lift forces to remain poorly understood. In this paper we present some results of an LBM study of the inertial migration of oblate spheroids in a plane channel, where steady laminar flow of moderate Re is generated by a pressure gradient. We perform measurements of the lift force acting on spheroids in the stable log-rolling regime and find that the lift coefficient depends only on their equatorial radius a . To interpret this result we develop a scaling theory and derive an expression for a lift force. Our scaling expression has a power to easily predict equilibrium positions of oblate spheroids in microfluidic channels.

Our paper is arranged as follows. In Sec. II we define our system and mention briefly some expressions for a lift force acting on a spherical particle. Sec. III describes details and parameters of simulations. Simulation results are discussed in Sec. IV. We then present scaling arguments leading to an expression for a lift force. We conclude in Sec V.

II. MODEL

We consider an oblate spheroid with an equatorial radius a and a polar radius $b < a$ in a pressure-driven flow between two parallel walls, separated by a distance H (see Fig. 1). Its location in the channel is defined by coordinates of the center $\mathbf{x} = (x, y, z)$ and by a unit vector directed along the symmetry axis $\mathbf{n} = (n_x, n_y, n_z)$ (referred below to as the orientation vector). At the channel walls and particle surface we apply no-slip boundary conditions.

The velocity profile in the channel in the absence of the particle is parabolic,

$$U(z) = 4U_m z(1 - z/H)/H, \quad (1)$$

where $U_m = |\nabla p|H^2/(8\mu)$ is the fluid velocity at the channel center, ∇p is a pressure gradient and μ is the dynamic viscosity. The (finite) channel Reynolds number $Re = \rho U_m H/\mu$, where ρ is the fluid density.

The inertial lift force drives particles across the flow streamlines. For spherical particles it can be written as^{5,7}

$$F_l(z) = \rho a^4 G_m^2 c_l, \quad (2)$$

where $G_m = 4U_m/H$ is the shear rate at the wall and c_l is the lift coefficient, given by

$$c_l = c_{l0} + V_s c_{l1} + V_s^2 c_{l2}, \quad (3)$$

where c_{li} , $i = 0, 1, 2$ are the lift coefficients that depend on the dimensionless particle position z/H , its size a/H , and Re . The dimensionless slip velocity is defined by

$$V_s = \frac{V_p^x - U(z)}{U_m}, \quad (4)$$

where V_p^x is the x -component of the particle velocity and U is the undisturbed fluid velocity at the particle center z . Note that it is normally considered that the slip velocity is induced by external forces only and, consequently, does not impact a hydrodynamic lift of neutrally buoyant particles. However, it has been recently shown that for neutrally buoyant particles V_s is negligibly small only in the central portion of the channel, but not near the wall, where it becomes finite⁷.

Eq.(2) is widely invoked to estimate the migration velocity of neutrally buoyant (of $\rho_p = \rho$) spherical particles¹³. When the lift force is balanced by the Dean¹³ or external^{26,27} force F_{ex} (in the case of non-neutrally buoyant particles, $\rho_p \neq \rho$), Eq.(2) can be applied to find the equilibrium positions, z_{eq} , using the force balance

$$F_l(z_{eq}) + F_{ex} = 0 \quad (5)$$

One normally assumes that $F_{ex} = V f_{ex}$, where $V = \frac{4}{3}\pi a^3$ is the volume of a sphere and f_{ex} is a force per unit volume. For instance, under the influence of gravity $f_{ex} = -(\rho_p - \rho)g$. In order to employ a similar approach to the shape-based separation of spheroids (of $V = \frac{4}{3}\pi a^2 b$) it is necessary to know how the lift force scales with the particle radii a and b , and with the aspect ratio b/a .

It is of considerable interest to obtain a similar scaling equation for spheroids. However, as described in the Introduction, their instantaneous orientation and rotation are often functions of time, which should lead to a time-dependent lift. Nevertheless, for neutrally-buoyant oblate spheroids of finite $Re_p = \rho G_m a^2/\mu$, the symmetry axis eventually becomes parallel to the vorticity direction, $\mathbf{n}_{eq} = (0, 1, 0)$ (the log-rolling motion). Consequently, to predict their long-term migration we have to find a lift force for this steady configuration. Once it is known, the equilibrium positions of oblate spheroids (including non-neutrally buoyant too) can be found by balancing the lift and external forces.

III. SIMULATION SETUP

To simulate fluid flow in the channel we use a 3D, 19 velocity, single relaxation time implementation of the lattice Boltzmann method (LBM) with a Batnagar Gross Krook (BGK) collision operator^{28,29}. Spheroids are discretized on the fluid lattice and implemented as moving no-slip boundaries following the pioneering work of Ladd¹⁸. Details of our implementation can be found in our previous publications^{7,29-33}.

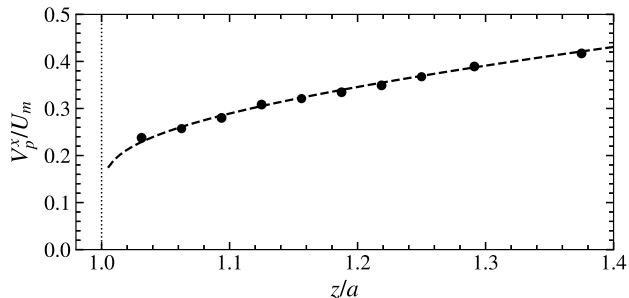


Figure 2. Velocity of a sphere of $a/H = 0.1$ located at a distance z from the wall and free to rotate and translate in the x -direction (circles). Dashed curve are calculations from Eq. (A8) representing the semi-analytical solution for a wall-bounded shear flow. Dotted line indicates a contact with the wall.

The size of the simulation domain is $(N_x, N_y, N_z) = (128, 128, 81)$, with corresponding channel height $H = 80$ (all units are simulation units). No-slip boundaries are implemented at the top and bottom channel walls using mid-grid bounce-back boundary conditions and all remaining boundaries are periodic. The kinematic viscosity is $\nu = 1/6$ and the fluid is initialized with a density $\rho = 1$. A body force directed along x with volumetric density $g = 0.5 \dots 2 \times 10^{-5}$ is applied both to the fluid and the particle, resulting in a Poiseuille flow with $\text{Re} \simeq 11 \dots 44$.

To simulate particle trajectories we use spheroids of equatorial radii $a = 6, 8$ and 12 and several aspect ratios, $0.33 \leq b/a \leq 1$. This range of particle aspect ratios is chosen to ensure the correct representation of ellipsoidal shape on the grid. The particles start close to the expected equilibrium with zero initial velocity and in log-rolling orientation. We assume that the equilibrium is reached when the difference between an average of particle z -coordinate over 10 time steps and its average over the next 10 step does not exceed $1.25 \times 10^{-6}H$.

To measure the lift force as a function of z , we fix particle z -coordinate but let to rotate and to move in all other directions. Particle motion starts with zero initial velocity and $\mathbf{n} = (0, 1, 0)$ that corresponds to the stable log-rolling state. Once a stationary velocity is reached, the vertical component of the force $F_l(z)$ is measured and is averaged over 10^4 simulation steps. Therefore, these measurements also correspond (if we neglect force fluctuations) to non-neutrally particles at equilibrium, Eq.(5).

To check if the results depend on the box size due to periodic boundary conditions in x - and y -directions, we also simulate the migration of the large sphere of $a = b = 12$ in a larger simulation box with $(N_x, N_y, N_z) = (256, 256, 81)$. The difference in equilibrium positions for the two box sizes is 100 times smaller than the typical separation of equilibrium positions of different particles.

To test the resolution of the method in the near-wall zone, we measure the velocity of the freely rotating and translating in x -direction sphere of radius $a = 8$, which z -coordinate is fixed. The x -component of the velocity V_p^x is plotted in Fig. 2,

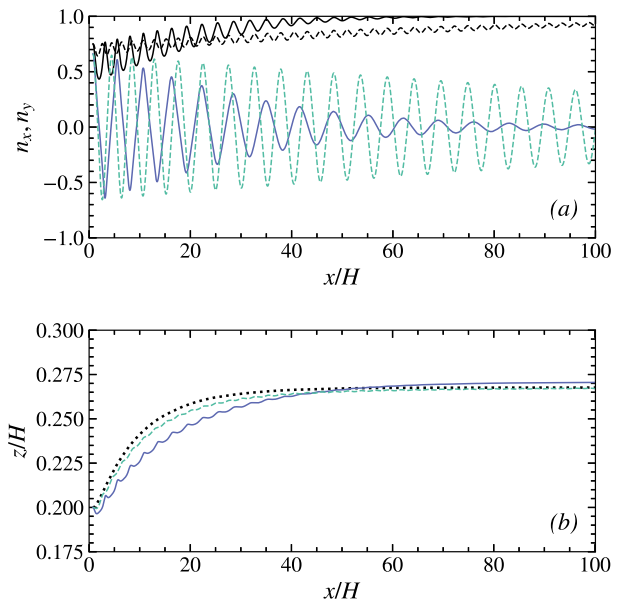


Figure 3. (a) x -components (colored curves) and y -components (black curves) of the orientation vector and (b) trajectories for spheroids with $a/H = 0.15$ and $b/a = 0.5$ (solid), 0.8 (dashed) and 1 (dotted).

along with a semi-analytical solution for a wall-bounded shear flow³⁴(see Eq. (A8)). One can see that a sufficient accuracy is attained for separations as small as 1 lattice nodes ($z/a > 1.05$), similarly to previous results for the sphere approaching a rough wall²⁹.

IV. NUMERICAL RESULTS AND DISCUSSION

We first simulate trajectories and orientations of freely moving neutrally buoyant spheroids of different sizes and aspect ratios in a flow with $\text{Re} = 22$. Our results show that regardless of the initial position and orientation, oblate spheroids eventually reorient to the stable log-rolling motion around the axis of symmetry and their angular velocity is directed along the y axis, $\mathbf{n} = (0, 1, 0)$, $\boldsymbol{\omega} = (0, \omega_y, 0)$. We also observe that they focus at some distance z_{eq} from the wall due to the inertial migration. The rates of reorientation and migration depend on the particle size and the aspect ratio.

In Fig. 3 we compare the rotational behavior and trajectories of spheroids of several aspect ratios, $b/a = 1$ (sphere), 0.8 and 0.5 , but of the same equatorial radius $a/H = 0.15$. For all simulations the initial position and orientation are fixed to $z_0/H = 0.2$ and $\mathbf{n}_0 = (0.66, 0.75, 0)$. It is well seen in Fig. 3(a) that the x -component of the orientation vector n_x experiences decaying oscillations around 0, while n_y converges to 1. This indicates that at the beginning particles exhibit a kayaking, which then slowly evolves to a log-rolling motion (see Fig. 1). Note that oscillations in the orientation of a spheroid with $b/a = 0.8$ decrease much slower than those for a spheroid of

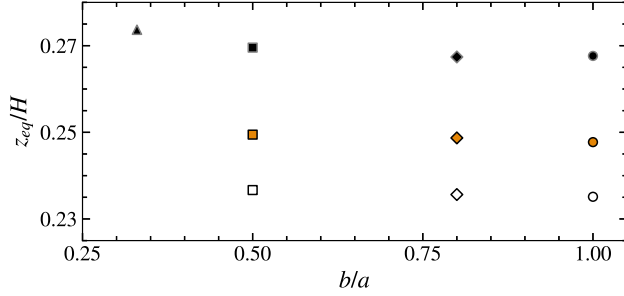


Figure 4. Equilibrium positions of spheroids with fixed $a/H = 0.075$, 0.1, 0.15 (open, colored, black symbols, respectively) vs. their aspect ratio.

$b/a = 0.5$. The kayaking motion is responsible for the oscillations in trajectories shown in Fig. 3(b). We see that for a spheroid of $b/a = 0.8$ the migration to the equilibrium position is faster than for that of $b/a = 0.5$, although the particle trajectory is much less affected by the kayaking motion. Another important observation is that the equilibrium positions for all spheroids are very close, pointing strongly that they are defined by the equatorial radius a . This result is consistent with reported experimental data^{10,11}. To validate this finding, below we compute z_{eq} for spheroids of different sizes and aspect ratios.

Let us now fix several a and simulate z_{eq} as a function of b/a . The results for a lower equilibrium position are plotted in Fig. 4. As expected, z_{eq} strongly depends on a , but is practically independent of the aspect ratio of spheroids. We stress that equilibrium positions are nearly independent of Re in the range from 11 to 44 used here. The same conclusion has been earlier made for spherical particles⁷.

Based on these observations, one can speculate that the lift coefficient at any, not only equilibrium, z is controlled by the equatorial radius. If so, we can suppose that the lift force on oblate spheroids of equatorial radius a represents a product of Eq. (2) for a sphere of the same radius and the correction f that depends on the aspect ratio

$$F_l = \rho a^4 G_m^2 c_l(z/H, a/H, Re) f(b/a). \quad (6)$$

This ansatz constitutes nothing more than an assumption, made to provide the lift force that depends on z only through the lift coefficient c_l .

To verify Eq. (6), we fix the z position of a spheroid that exhibits a stable log-rolling motion but is free to also translate in two other directions, and measure the lift force. If the form of ansatz (6) is correct, the ratio $F_l / (\rho a^4 G_m^2 c_l)$ would be equal to $f(b/a)$. In Fig. 5 we plot this ratio as a function of the particle position and conclude that for a given b/a it is nearly constant. Moreover, we see that $f \simeq b/a$. Note that results displayed in Fig. 5 correspond to $Re = 22$, but these conclusions have been verified for $Re = 11$ and 44 (not shown). Therefore, one can rewrite Eq.(6) as

$$F_l = \rho a^3 b G_m^2 c_l(z/H, a/H, Re). \quad (7)$$

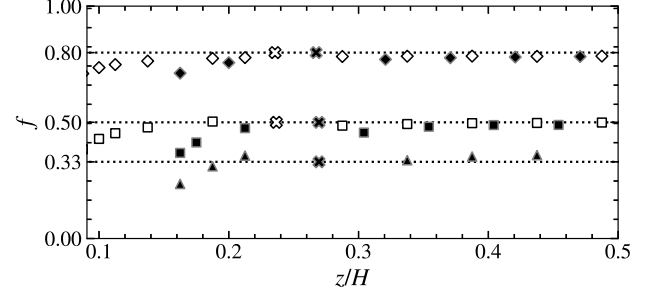


Figure 5. Ratio of the lift forces for spheroids and spheres of the same a computed at $Re = 22$ using $a/H = 0.075$ (open symbols) and 0.15 (black symbols). The aspect ratio b/a of spheroids in simulations is set to be equal to 0.33 (triangles), 0.5 (squares), and 0.8 (diamonds). Equilibrium positions of spheroids are marked by open ($a/H = 0.075$) and black ($a/H = 0.15$) crosses. Dotted lines show $f = b/a$.

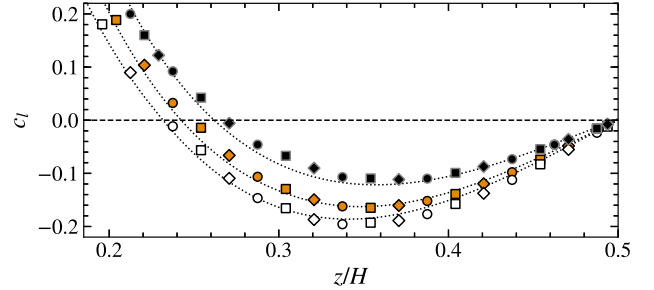


Figure 6. Lift coefficients, Eq. (7), in the channel central portion of the channel at $Re = 22$ computed using $a/H = 0.075$, 0.1, and 0.15 (open, colored, black symbols, respectively). The aspect ratio b/a is equal to 0.5 (squares), 0.8 (diamonds) and 1 (circles). Dotted curves show calculations from Eq.(3) using Eqs.(A1)-(A3) for c_{li} .

Eq.(7) allows one to obtain c_l from the simulation data simply by computing the ratio $F_l / (\rho a^3 b G_m^2)$, which is expected to depend on a/H , but not on the spheroid aspect ratio. We now calculate c_l for a sphere and spheroids of two aspect ratios (0.5 and 0.8, as before) using several values of a/H . The simulation results for the central region of the channel, $0.2 \leq z/H \leq 0.5$ are given in Fig. 6, which fully confirms that at fixed a/H the lift coefficient indeed does not depend on b/a . Using these simulation results in Appendix A we propose fitting expressions for the lift coefficient. Calculations from Eq.(3) using c_{li} given by Eqs.(A1)-(A3) are also included in Fig. 6, and we see that they fit well the simulation data. The overall conclusion from this plot is that our scaling Eq.(7) adequately describes the lift force in the central region of the channel.

However, as seen in Fig. 7(a), Eq.(7) becomes inaccurate very close to the wall, namely, when $z - a \leq 0.2a$. At such small distances between spheroids and the wall the lift coefficient is no longer independent of the aspect ratio, and we see

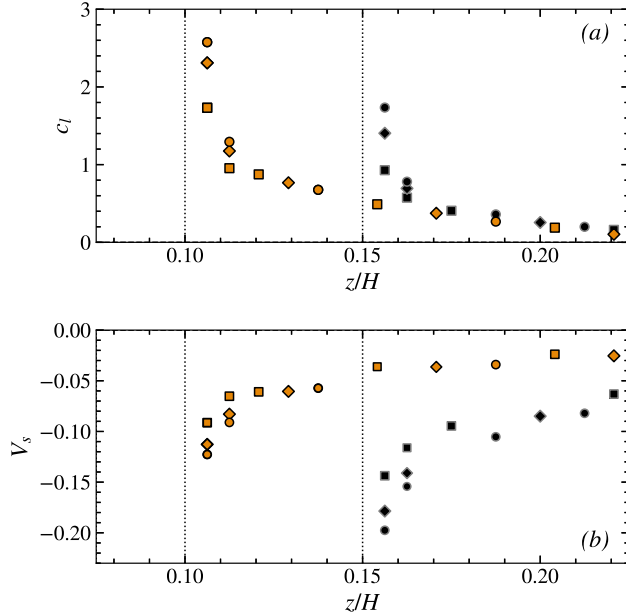


Figure 7. (a) Lift coefficient and (b) particle slip velocity near the wall for spheroids of $b/a = 0.5$ (squares), 0.8 (diamonds) and spheres (circles). Colored and black symbols correspond to $a/H = 0.1$ and 0.15 . Dotted lines indicate a contact with the wall.

that c_l augments with b/a . An explanation for the smaller c_l for the spheroids compared to the sphere can be obtained if we invoke their hydrodynamic interactions with the wall that depends on both a and b ³⁵. This is illustrated and confirmed in Fig. 7(b), where the data for the particle slip velocity near the wall are presented. It is well seen that close to the wall V_s is finite and varies with both a and b/a . More oblate particles have a smaller slip velocity and, therefore, experience a smaller lift force.

Additional insight into the problem can be gleaned by computing the equilibrium positions for particles of an equal volume V , but of various aspect ratio. This situation is relevant to separation experiments^{10,11}. We now fix a^2b , so that it is equivalent of that for a sphere of $a/H = 0.1$, and measure z_{eq} at $Re = 22$ and different b/a . Simulation results for neutrally-buoyant oblate spheroids are included in Fig. 8 (black symbols). It is seen that a decrease in b/a has the effect of larger z/H , although rather insignificant. Since the lift coefficient and z_{eq} (where c_l vanishes) are independent of b as follows from Eq. (7), the weak variations of z_{eq} with the aspect ratio are caused by the changes in values of a . Fig. 8 also includes the data obtained by Lashgari *et al.*²⁴ by means of the LBM simulations at $Re = 50$ (shown by stars). We see that their results agree well with our simulations thus confirming that at moderate Re the equilibrium positions do not depend on its values. Finally, we note that calculations from Eq.(7) using Eq. (3) for c_l and Eqs.(A1)-(A3) for c_{li} fit the simulation data very well (solid curve).

These simulations are compared with analogous, made with the same parameters, but in which $\rho_p \neq \rho$ and an external

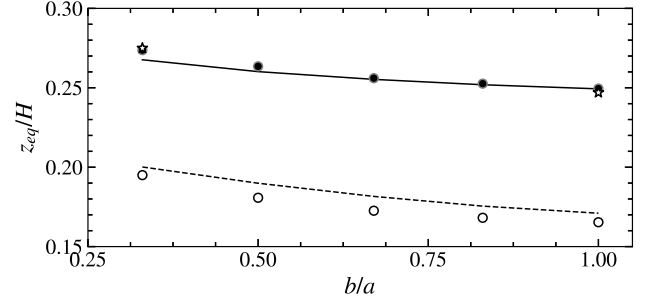


Figure 8. Equilibrium positions for spheroids of the same volume (equivalent to that of a sphere of $a/H = 0.1$) vs. the aspect ratio obtained in simulations at $Re = 22$ (circles). Black circles indicate neutrally buoyant spheroids, open circles show results for non-neutrally buoyant spheroids subject to an external force ($c_{ex} = -0.045$). Stars show the simulation data by Lashgari *et al.*²⁴ obtained at $Re = 50$. Solid and dashed curves are calculations from Eqs. (7) and (8). In both cases Eq. (3) and Eqs.(A1)-(A3) are used to calculate c_l and c_{li} .

force is incorporated. The equilibrium positions of such non-neutrally buoyant spheroids have been found from

$$c_l(z_{eq}/H, a/H, Re) = -\frac{c_{ex}H}{a}, \quad (8)$$

obtained by using Eq.(5) together with Eq. (7), where the dimensionless parameter c_{ex} that characterizes the relative value of the external force is given by

$$c_{ex} = \frac{4\pi f_{ex}}{3\rho G_m^2 H}. \quad (9)$$

Since Eq.(8) does not include b , at constant f_{ex} the equilibrium positions for particles of the same a coincide. Simulations made with $c_{ex} = -0.045$ are included in Fig. 8 (open symbols) and show that z_{eq}/H are shifted towards the bottom wall compared to neutrally buoyant spheroids. Note that with our parameters Eq. (8) has only one root, so that the upper equilibrium position cannot be attained. Also included in Fig. 8 are the calculations from Eq. (8), where c_l is obtained using Eq.(3) with c_{li} given by (A1)-(A3) (dashed curve). We see that they are in a good agreement with the simulation results.

V. CONCLUSION

We have presented lattice Boltzmann simulation data on the inertial migration of oblate spheroids in the channel flow with moderate Reynolds numbers. Our results show that spheroids focus to equilibrium positions, which depend only on their equatorial radius a , but not on the polar radius b . We invoke this simulation result to derive a scaling expression for a lift force, Eq.(7). In this expression, the lift force is proportional to a^3b , but the lift coefficient, c_l , is the same as for a sphere of radius a . We have also proposed fitting expressions allowing one to easily calculate c_l . Our scaling theory is shown to be valid throughout the channel, except very narrow regions

near a wall. Thus, it can be employed to predict, with high accuracy, the equilibrium positions of spheroids in the channel. These, in turn, could be used to develop inertial microfluidic methods for a shape-based separation.

We recall, that in our work we have limited ourselves by oblate spheroids of $b/a \geq 0.3$ and used $Re \leq 44$ only, but one cannot exclude that at lower aspect ratios and/or larger Reynolds numbers the equilibrium positions would depend on both radii of particles. It would be of considerable interest to explore the validity of Eq. (7) using other flow and oblate spheroid parameters. Another fruitful direction could be an investigation of prolate particles to develop an analogue of Eq. (7).

ACKNOWLEDGMENTS

This research was partly supported by the Russian Foundation for Basic Research (grant 18-01-00729), by the Ministry of Science and Higher Education of the Russian Federation and by the German Research Foundation (research unit FOR2688, project HA4382/8-1).

DATA AVAILABILITY STATEMENT

The data that support the findings of this study are available within the article.

Appendix A: Fitting expressions for the lift coefficients and particle velocity

The lift coefficient for the sphere is given by Eq.(3) and depends on the coefficients c_{li} and on the slip velocity V_s . The later is defined by Eq.(4) and depends on the particle velocity V_p^x . Consequently, to apply Eq.(7) for oblate spheroids we have to determine c_{li} and V_p^x for a sphere. In this Appendix we propose some useful fitting expressions for these functions.

We propose a modification of expressions for c_{li} reported by Asmolov *et al.*⁷

$$c_{l0} = \beta_0(a/H)c_{l0}^{VC}(z/H), \quad (\text{A1})$$

$$c_{l1} = 4(1 - 2z/H)\beta_1(a/H)c_{l1}^{CM}(z/a), \quad (\text{A2})$$

$$c_{l2} = c_{l2}^{CM}(z/a), \quad (\text{A3})$$

where correction factors β_0 and β_1 allow for fitting the data for bigger particles then before. By fitting our simulation data for several a/H (see Sec. IV) we obtain

$$\begin{aligned} \beta_0 &= 1 + 3.32(a/H) - 26.45(a/H)^2, \\ \beta_1 &= 1 - 8.39(a/H) + 19.65(a/H)^2. \end{aligned} \quad (\text{A4})$$

The coefficient c_{l0}^{VC} in Eq.(A1) represents the analytical solution by Vasseur and Cox³⁶ for pointlike spherical particles in the low Re channel flow, which can be well fitted by

$$c_{l0}^{VC} = 2.25(z/H - 0.5) - 23.4(z/H - 0.5)^3. \quad (\text{A5})$$

as suggested by Feuillebois³⁷. The coefficients c_{l1}^{CM} and c_{l2}^{CM} in Eqs.(A2) and (A3) are these obtained by Cherukat and McLaughlin^{38,39} for finite-size particles in a near-wall shear flow

$$c_{l1}^{CM} = -3.2415\zeta - 2.6729 - 0.8373\zeta^{-1} + 0.4683\zeta^{-2}, \quad (\text{A6})$$

$$c_{l2}^{CM} = 1.8065 + 0.89934\zeta^{-1} - 1.961\zeta^{-2} + 1.02161\zeta^{-3}, \quad (\text{A7})$$

where $\zeta = z/a$.

At relatively large distances from the wall, the particle slip velocity (and, hence, V_p^x) is independent of b and, unlike wall-bounded shear flow, remains finite (see Fig. 7). Therefore, for this central region one can use the approximation for the sphere of radius a . The velocity V_p^x can be presented as a sum of the solution for a wall-bounded linear shear flow^{34,40}

$$V_l^x = U(z)h(z/a), \quad (\text{A8})$$

with

$$h = \frac{200.9\xi - (115.7\xi + 721)\zeta^{-1} - 781.1}{-27.25\xi^2 + 398.4\xi - 1182} \quad \text{at } \zeta < 3, \quad (\text{A9})$$

$$h = \frac{1 - \frac{5}{4}\zeta^{-3} + \frac{5}{4}\zeta^{-5} - \frac{23}{48}\zeta^{-7} - \frac{1375}{1024}\zeta^{-8}}{1 - \frac{15}{16}\zeta^{-3} + \zeta^{-5} - \frac{3}{8}\zeta^{-7} - \frac{4565}{4096}\zeta^{-8}} \quad \text{at } \zeta \geq 3, \quad (\text{A10})$$

where $\xi = \log(\zeta - 1)$, and the Faxen correction due to the parabolic flow profile:

$$V_p^x = V_l^x - 4/3(a/H)^2. \quad (\text{A11})$$

REFERENCES

- ¹J. Zhang, S. Yan, D. Yuan, G. Alici, N.-T. Nguyen, M. E. Warkiani, and W. Li, "Fundamentals and applications of inertial microfluidics: a review," *Lab. Chip* **16**, 10–34 (2016).
- ²D. Stoecklein and D. Di Carlo, "Nonlinear microfluidics," *Anal. Chem.* **91**, 296–314 (2019).
- ³G. Segre and A. Silberberg, "Behaviour of macroscopic rigid spheres in Poiseuille flow. Part I. Determination of local concentration by statistical analysis of particle passages through crossed light beams," *J. Fluid Mech.* **14**, 115–135 (1962).
- ⁴P. Vasseur and R. G. Cox, "The lateral migration of spherical particles sedimenting in a stagnant bounded fluid," *J. Fluid Mech.* **80**, 561–591 (1977).
- ⁵E. S. Asmolov, "The inertial lift on a spherical particle in a plane Poiseuille flow at large channel Reynolds number," *J. Fluid Mech.* **381**, 63–87 (1999).
- ⁶K. Hood, S. Lee, and M. Roper, "Inertial migration of a rigid sphere in three-dimensional Poiseuille flow," *J. Fluid Mech.* **765**, 452–479 (2015).
- ⁷E. S. Asmolov, A. L. Dubov, T. V. Nizkaya, J. Harting, and O. I. Vinogradova, "Inertial focusing of finite-size particles in microchannels," *J. Fluid Mech.* **840**, 613–630 (2018).
- ⁸D. Di Carlo, J. F. Edd, K. J. Humphry, H. A. Stone, and M. Toner, "Particle segregation and dynamics in confined flows," *Phys. Rev. Lett.* **102**, 094503 (2009).
- ⁹B. Behdani, S. Monjezi, M. J. Carey, C. G. Weldon, J. Zhang, C. Wang, and J. Park, "Shape-based separation of micro-/nanoparticles in liquid phases," *Biomicrofluidics* **12**, 051503 (2018).
- ¹⁰S. C. Hur, S.-E. Choi, S. Kwon, and D. D. Carlo, "Inertial focusing of non-spherical microparticles," *Appl. Phys. Lett.* **99**, 044101 (2011).

- ¹¹M. Masaeli, E. Sollier, H. Amini, W. Mao, K. Camacho, N. Doshi, S. Mitra, A. Alexeev, and D. Di Carlo, “Continuous inertial focusing and separation of particles by shape,” *Phys. Rev. X* **2**, 031017 (2012).
- ¹²T. Roth, L. Sprenger, S. Odenbach, and U. O. Haefeli, “Continuous form-dependent focusing of non-spherical microparticles in a highly diluted suspension with the help of microfluidic spirals,” *Phys. Fluids* **30**, 045102 (2018).
- ¹³D. Di Carlo, D. Irimia, R. Tompkins, and M. Toner, “Continuous inertial focusing, ordering, and separation of particles in microchannels,” *PNAS* **104**, 18892–18897 (2007).
- ¹⁴J. Su, X. Chen, and G. Hu, “Inertial migrations of cylindrical particles in rectangular microchannels: Variations of equilibrium positions and equivalent diameters,” *Phys. Fluids* **30**, 032007 (2018).
- ¹⁵G. Jeffrey, “The motion of ellipsoidal particles immersed in a viscous fluid,” *Proc. R. Soc. A* **82**, 161–179 (1922).
- ¹⁶P. G. Saffman, “On the motion of small spheroidal particles in a viscous liquid,” *J. Fluid Mech.* **1**, 540–553 (1956).
- ¹⁷S. R. Bazaz, A. Mashhadian, A. Ehsani, S. C. Saha, T. Krüger, and M. E. Warkiani, “Computational inertial microfluidics: a review,” *Lab. Chip* **20**, 1023–1048 (2020).
- ¹⁸A. J. C. Ladd and R. Verberg, “Lattice-Boltzmann simulations of particle-fluid suspensions,” *J. Stat. Phys.* **104**, 1191 (2001).
- ¹⁹D. Qi and L.-S. Luo, “Rotational and orientational behaviour of three-dimensional spheroidal particles in Couette flows,” *J. Fluid Mech.* **477**, 201–213 (2003).
- ²⁰F. Janoschek, F. Mancini, J. Harting, and F. Toschi, “Rotational behavior of red blood cells in suspension: a mesoscale simulation study,” *Phil. Trans. R. Soc. London Series A* **369**, 2337–2344 (2011).
- ²¹T. Rosén, F. Lundell, and C. Aidun, “Effect of fluid inertia on the dynamics and scaling of neutrally buoyant particles in shear flow,” *J. Fluid Mech.* **738**, 563–590 (2014).
- ²²H. Huang and X.-Y. Lu, “An ellipsoidal particle in tube poiseuille flow,” *J. Fluid Mech.* **822**, 664–688 (2017).
- ²³M. Li, H. E. Muñoz, K. Goda, and D. Di Carlo, “Shape-based separation of microalga *euglena gracilis* using inertial microfluidics,” *Sci Rep* **7**, 1–8 (2017).
- ²⁴I. Lashgari, M. N. Ardekani, I. Banerjee, A. Russom, and L. Brandt, “Inertial migration of spherical and oblate particles in straight ducts,” *J. Fluid Mech.* **819**, 540–561 (2017).
- ²⁵Y. Huang, R. L. Marson, and R. G. Larson, “Inertial migration of neutrally buoyant prolate and oblate spheroids in plane Poiseuille flow using dissipative particle dynamics simulations,” *Comput. Mater. Sci.* **162**, 178–185 (2019).
- ²⁶J. Zhang, S. Yan, G. Alici, N.-T. Nguyen, D. Di Carlo, and W. Li, “Real-time control of inertial focusing in microfluidics using dielectrophoresis (dep),” *RSC Adv.* **4**, 62076–62085 (2014).
- ²⁷S. Dutz, M. Hayden, and U. Häfeli, “Fractionation of magnetic microspheres in a microfluidic spiral: Interplay between magnetic and hydrodynamic forces,” *PloS one* **12**, e0169919 (2017).
- ²⁸R. Benzi, S. Succi, and M. Vergassola, “The lattice Boltzmann equation: theory and applications,” *Physics Reports* **222**, 145 (1992).
- ²⁹C. Kunert, J. Harting, and O. I. Vinogradova, “Random-roughness hydrodynamic boundary conditions,” *Phys. Rev. Lett.* **105**, 016001 (2010).
- ³⁰F. Janoschek, F. Toschi, and J. Harting, “Simplified particulate model for coarse-grained hemodynamics simulations,” *Phys. Rev. E* **82**, 056710 (2010).
- ³¹F. Janoschek, J. Harting, and F. Toschi, “Towards a continuum model for particle-induced velocity fluctuations in suspension flow through a stenosed geometry,” *Int. J. Modern Physics C* **25**, 1441013 (2014).
- ³²A. L. Dubov, S. Schmieschek, E. S. Asmolov, J. Harting, and O. Vinogradova, “Lattice-Boltzmann simulations of the drag force on a sphere approaching a superhydrophobic striped plane,” *J. Chem. Phys.* **140**, 034707 (2014).
- ³³T. V. Nizkaya, E. S. Asmolov, J. Harting, and O. I. Vinogradova, “Inertial migration of neutrally buoyant particles in superhydrophobic channels,” *Phys. Rev. Fluids* **5**, 014201 (2020).
- ³⁴P. Reschiglian, D. Melucci, G. Torsi, and A. Zattoni, “Standardless method for quantitative particle-size distribution studies by gravitational field-flow fractionation. application to silica particles,” *Chromatographia* **51**, 87–94 (2000).
- ³⁵O. I. Vinogradova, “Hydrodynamic interaction of curved bodies allowing slip on their surfaces,” *Langmuir* **12**, 5963–5968 (1996).
- ³⁶P. Vasseur and R. G. Cox, “The lateral migration of a spherical particle in two-dimensional shear flows,” *J. Fluid Mech.* **78**, 385–413 (1976).
- ³⁷F. Feuillebois, “Perturbation problems at low Reynolds number,” *Lecture Notes-AMAS* (2004).
- ³⁸P. Cherukat and J. B. McLaughlin, “The inertial lift on a rigid sphere in a linear shear flow field near a flat wall,” *J. Fluid Mech.* **263**, 1–18 (1994).
- ³⁹P. Cherukat and J. B. McLaughlin, “The inertial lift on a rigid sphere in a linear shear flow field near a flat wall. Corrigendum,” *J. Fluid Mech.* **285**, 407 (1995).
- ⁴⁰S. Wakiya, C. Darabaner, and S. Mason, “Particle motions in sheared suspensions XXI: Interactions of rigid spheres (theoretical),” *Rheol. Acta* **6**, 264–273 (1967).